Photojunction Field-Effect Transistor Based on a Colloidal Quantum Dot Absorber Channel Layer

Valerio Adinolfi, Illan J. Kramer, André J. Labelle, Brandon R. Sutherland, S. Hoogland, and Edward H. Sargent*

Department of Electrical Engineering and Computer Science, University of Toronto, 10 King's College Road, Toronto, Ontario M5S 3G4, Canada

ABSTRACT The performance of photodetectors is judged via high responsivity, fast speed of response, and low background current. Many previously reported photodetectors based on size-tuned colloidal quantum dots (CQDs) have relied either on photodiodes, which, since they are primary photocarrier devices, lack gain; or photoconductors, which provide gain but at the expense of slow response (due to delayed charge carrier escape from sensitizing centers) and an inherent dark current vs responsivity trade-off. Here we report a photojunction field-effect transistor (photoJFET), which provides gain while breaking prior photoconductors' response/speed/dark current trade-off. This is achieved by ensuring that, in the dark, the channel is fully depleted due to a rectifying junction between a deep-work-function transparent conductive top contact (MoO_3) and a moderately n-type CQD film (iodine treated PbS CQDs). We characterize the rectifying behavior of the junction and the linearity of the channel characteristics under illumination, and we observe a 10 μs rise time, a record for a gain-providing, low-dark-current CQD photodetector. We prove, using an analytical model validated using experimental measurements, that for a given response time the device provides a two-orders-of-magnitude improvement in photocurrent-to-dark-current ratio compared to photoconductors. The photoJFET, which relies on a junction gate-effect, enriches the growing family of CQD photosensitive transistors.

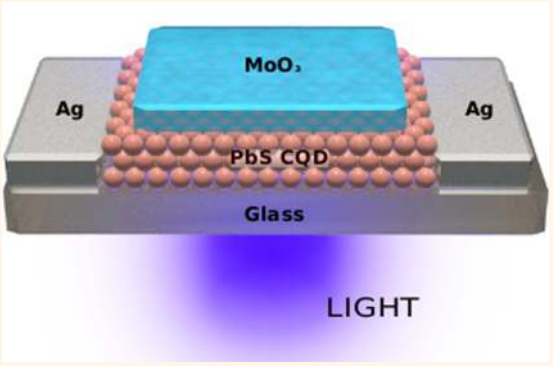

KEYWORDS: colloidal quantum dots · photodetectors · FET · phototransistors · JFET

Light sensors, crucial to image capture, optical communications, and biophotonics, have until recently been built principally using single-crystal semiconductor materials such as Si, GaAs, and InGaAs.[1−3] Recently, significant strides have been made in producing solution-processed light sensors based instead on soft materials. These hold the advantage of reduced manufacturing cost as well as compatibility—without concern for lattice-match—with a wide array of possible substrates, including curved and flexible ones.[4−6]

Colloidal quantum dots are an example of one such solution-processed optoelectronic material.[7] In addition to low cost and substrate compatibility, they also provide quantum size effect tuning, wherein the bandgap, and hence the spectral onset of light absorption, can be programmed at the time of fabrication by controlling the nanoparticle diameter.[8,9]

Two main classes of CQD photodetectors have seen much attention. The first, photodiodes, rely on rectifying junctions and generally provide low dark currents and high operating frequencies.[10] Indeed fast-responding CQD photodiodes have provided 3 dB frequencies in excess of 1 MHz.[11] The other class of widely explored photodetectors are photoconductors.[12,13] These offer the advantage of photoconductive gain, which can produce a large number of electrons of photocurrent collected for each absorbed photon. This upfront gain facilitates subsequent processing of analog signals. It generally comes at a penalty to both speed and dark current.[14,15]

A different class of light detectors, phototransistors, combines gain and a transistor effect. These have attracted attention[16−18] since they combine impressive signal amplification with a reasonable response time.[19,20] In this work, we investigate a photojunction

* Address correspondence to ted.sargent@utoronto.ca.

Received for review September 21, 2014 and accepted January 5, 2015.

Published online January 05, 2015
10.1021/nn5053537

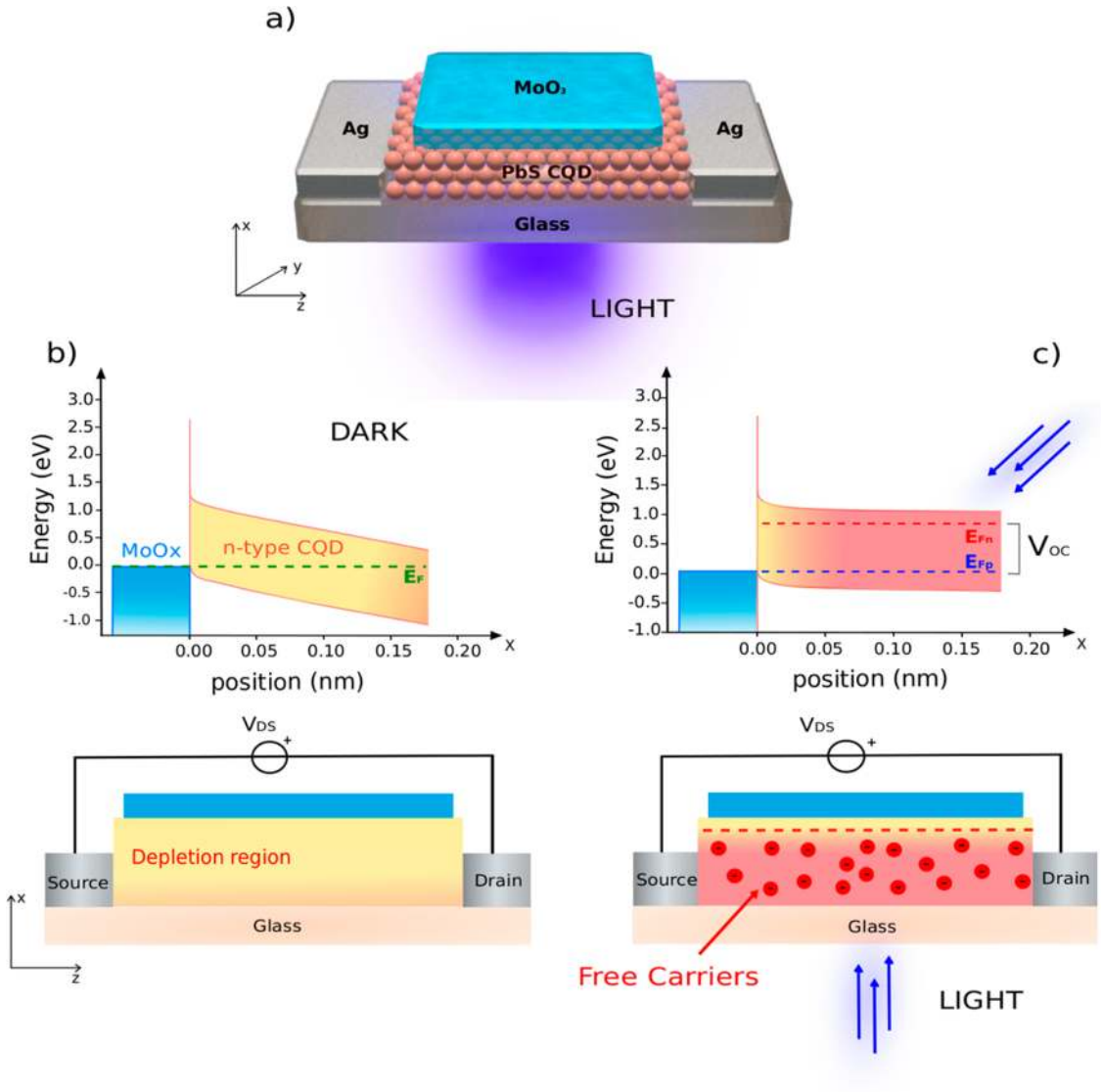

Figure 1. (a) Schematic of the photoJFET. CQDs are deposited on glass and contacted with silver source and drain contacts. A layer of MoO_3 is deposited on top of the CQD layer. The sample is illuminated through the glass substrate. Simulated energy band diagrams of (b, top) dark and (c, top) illuminated photoJFETs. The fully depleted device (b, bottom) exhibits bent bands and reduced free carriers, whereas illumination (in this case λ = 450 nm) generates an open-circuit voltage and a large population of free carriers (c, bottom). The new band alignment results in a CQD channel replenished of free carriers (electrons) due to the shrinkage of the depletion region.

field-effect transistor, or photoJFET. Our concept is described in Figure 1. As in a JFET,[21] the conductance of a channel is modulated by a change in the density of free charge carriers; and this conductance is sensed using a lateral source−drain connection to the channel. Also in common with the conventional JFET, the photoJFET is a junction device in the direction orthogonal to the channel flow direction. In the present case, a rectifying junction between a deep work function transparent conductor (MoO_3) and the normally n-type channel semiconductor, a CQD solid, produces a normally depleted (normally off) channel. Molybdenum trioxide has previously been employed as a back ohmic contact in the best-performing reported CQD solar cells.[22] In contrast with the conventional JFET, the photoJFET exploits light-induced, instead of externally applied field-induced, modulation of the channel conductance.[23]

RESULTS AND DISCUSSION

Spatial band diagrams (Figure 1b,c) illustrate the operation of the photoJFET in the dark and under illumination. In the dark, the channel is fully depleted, thanks to a built-in potential due to the work function difference between the MoO_3 (Φ = 5.4 eV)[24−26] top contact and the n-doped PbS CQDs CQD film (Φ = 4.2 eV), combined with the relatively low doping of the CQD layer ($n_0 \approx N_D \approx 10^{16}$ cm^{-3})[27] and the judicious choice of CQD layer thickness (240−300 nm). We designed the channel for full depletion in the dark with the goal of minimizing dark current. This strategy is necessary because of

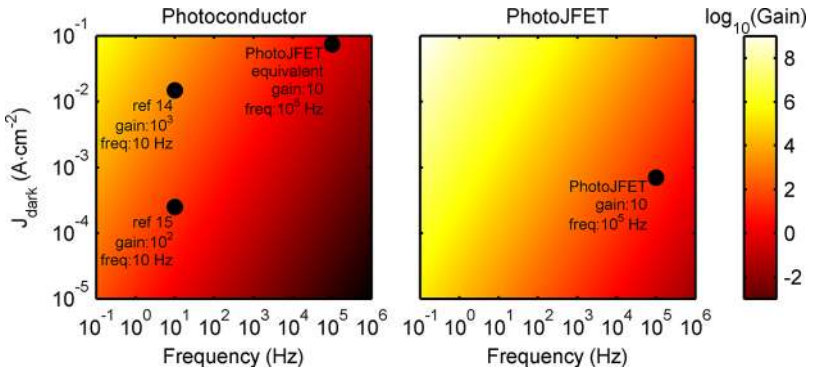

Figure 2. Analytical comparison between the photoJFET and a traditional photoconductor. Gain is plotted, using a color code, as a function of the dark current density and the maximum frequency of operation. The photoconductor shows warm colors in the top left corner of the plot, area corresponding to low frequency and high dark current. The photoJFET, instead, exhibits similar gain at much lower dark current and higher frequency. Previous reported devices and the equivalent performance photoconductor are positioned in the plot for comparison.

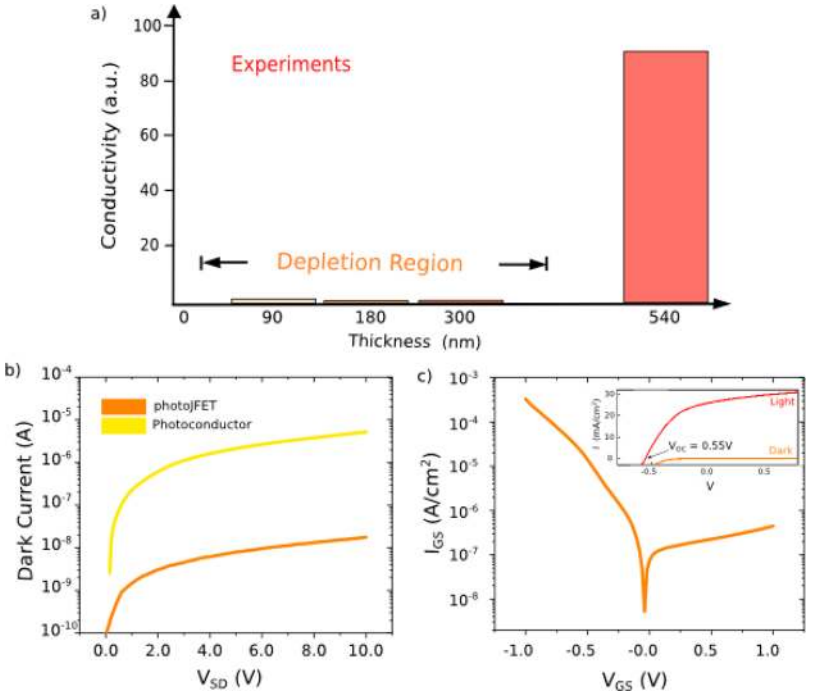

Figure 3. Experimental investigation on the operation of the photoJFET. (a) PhotoJFETs with different PbS CQD film thicknesses are investigated in terms of dark current. Up to a thickness 300 nm, the channel is fully depleted resulting in very low channel conductivity. When the CQD layer thickness exceeds the depletion width, the conductivity of the channel has a rapid increase as a result of the free carriers present in the CQD solid. (b) The quantitative comparison, in terms of dark current, between the photoJFET and a photoconductor (*i.e.*, pure CQDs) having the same thickness (150 nm). The photoJFET is able to reduce the current by 2 orders of magnitude. (c) The MoO_3/CQD rectifying IV curve is shown in dark and under AM 1.5 solar illumination (inset).

the absence of a high quality, highly intrinsic CQD solid.

Under illumination, the vertical MoO_3:CQD junction can be pictured as a Schottky device operating under open-circuit conditions (since the CQD film sits atop an insulator, glass, and is contacted with a floating top electrode). As seen in Figure 1c, under illumination with above-bandgap photons, the quasi-Fermi levels separate, with photoholes drawn toward the MoO_3 and photoelectrons filling the channel, with the light-absorption-driven emergence of a majority free electron density beginning at the bottom of the channel, *i.e.*, near the insulating substrate.

We investigate the prospective benefits of the photoJFET by first describing the results of analytical modeling presented in Figure 2 and detailed in the Supporting Information. In the photoconductor, photocarriers generated due to photon absorption will recirculate in the channel τ_l/τ_t times,[28] producing photoconductive gain, where τ_t is the transit time $\tau_t = L^2/\mu V$, τ_l is the carrier lifetime, L is the contact spacing, and V is the applied voltage. These considerations

highlight the inherent trade-off in photoconductors between gain and speed. While this trade-off can be made by increasing transport to decrease transit time, this results directly in an increase in dark current: $J_{dark} = qn_0L/\tau_t$.

In contrast, while the photoJFET also achieves gain as a ratio of excited state lifetime to transit time, the dark current of the photoJFET can be much lower than in the photoconductor since it is fully depleted in the dark. With this solution, a desirably small τ_t can be obtained without unacceptably increasing the dark current.

The breaking of the response/speed/dark current trade-off in the photoJFET relative to the photoconductor is illustrated in the example of Figure 2. For a given choice of device structural and materials parameters (Supporting Information), the photoJFET can achieve useful gain of 10, modulation frequency of 100 kHz, and a dark current fully 2 orders of magnitude lower compared to a photoconductor at the same gain and response speed.

We built a suite of phototransistors and characterized them to understand their operation and reveal their performance. Our first step was to experimentally find a channel thickness that would maximize light absorption but preserve fully depleted operation. As seen in Figure 3a, we can make a channel as thick as 300 nm and still achieve low dark current, consistent with theoretical estimates of the single-sided junction depletion region thickness for a $\sim 10^{16}$ cm^{-3} doped n-layer, $V_{bi} = 0.9$ V, and $\epsilon_r = 22$ ($x_d = ((2\varepsilon V_{bi})/(qN_d))^{1/2} \cong$ 460 nm).[29]

We next characterized the MoO_3:CQD vertical junction (Figure 3b). This axis of the device exhibits a rectification ratio as high as 10^4 and confirms that a highly asymmetric junction is indeed formed. The low leakage of the reverse-biased MoO_3:CQD junction is crucial to maintaining low dark current in the photoJFET in its intended operation mode.

Figure 3c compares the measured dark current. Characterization of a photoJFET and a photoconductor, each in the dark, reveals the advantage of using the fully depleted channel. A two-orders-of-magnitude advantage in dark current is maintained for all source–drain biases (V_{SD}) for the photoJFET relative to the photoconductor.

To characterize the device further, we acquired three figures of merit of interest in photodetection.[30] In Figure 4a we present the photocurrent spectrum, normalized to the response at 950 nm (the excitonic peak). The photocurrent response spectrum follows the absorption spectrum of the quantum dots closely, confirming the CQD solid's role in photocarrier generation and photoJFET photocurrent.

The device achieves a gain as high as 9.8 under low optical intensity (Figure 4b); this value decreases as superlinear recombination mechanisms (*e.g.*, bimolecular) take over at higher photogeneration rates.[23,31]

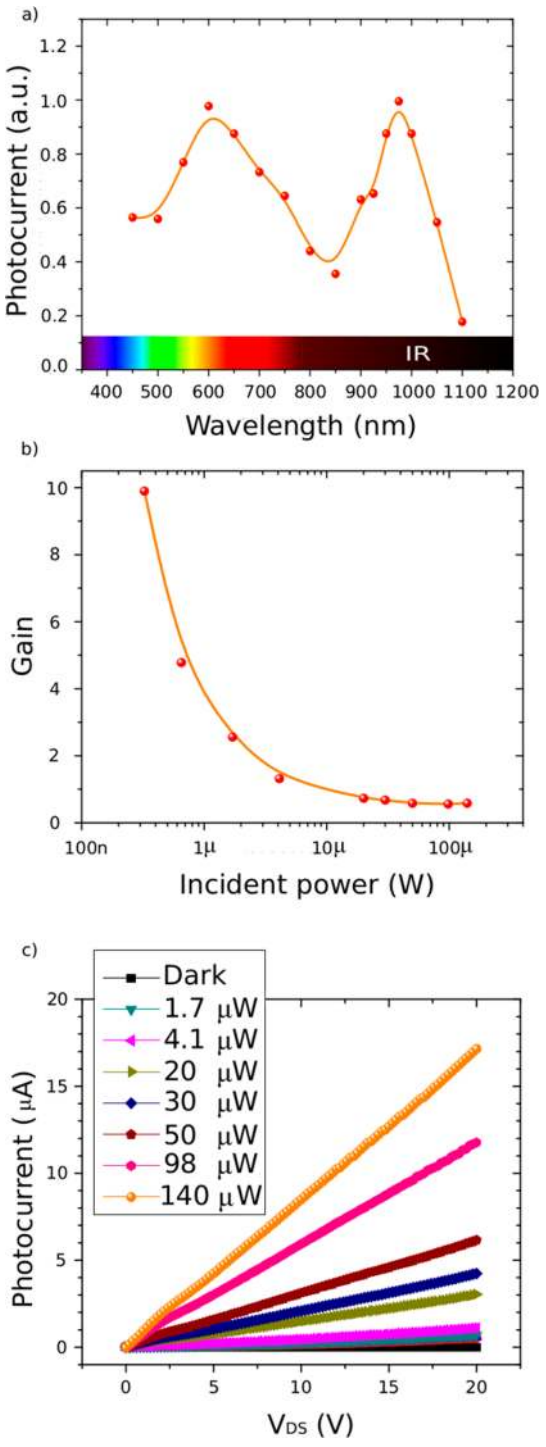

Figure 4. Electro-optical characterization of the photoJFET. (a) The spectral photocurrent is measured for a source–drain voltage of 5 V under a constant incident light power of 632 pW chopped at a frequency of 20 Hz. The plot shows a clear exciton peak around 950 nm matching the absorption profile of the PbS CQD semiconductor (see Supporting Information) demonstrating excellent photocarrier extraction through all the visible and NIR spectrum. (b) The gain is measured under a 30 V bias, monochromatic blue light excitation (λ = 450 nm) as a function of the incident light power. At low power the photoJFET reaches a gain of 9.8. (c) The photocurrent as a function of bias and incident light power is shown.

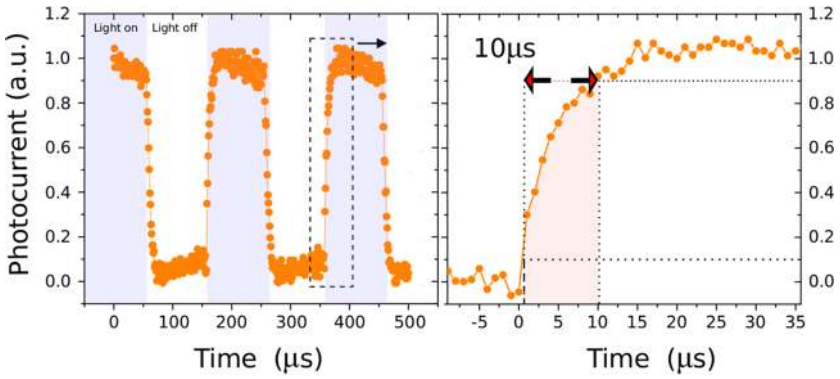

Figure 5. Speed characterization of the photoJFET. Transient photocurrent stimulated from a square wave modulated monochromatic light excitation (450 nm) is shown (left). A magnification of the rising edge, corresponding to the light response, reveals a response time (rise time from 10 to 90% of the full wave amplitude) of ~10 μs (right). The falling edge is characterized by the same time constant (see Supporting Information).

The measured value of the gain agrees well with the theoretical value estimated using the mobility and the carrier lifetime of the CQD film (the measurements and the analysis are included in the Supporting Information). The transfer characteristic of the source–drain current vs voltage is linear at all light levels studied, consistent with ohmic contact of the silver source and drain contacts to the n-type channel CQD film. Responsivity, noise current, and detectivity have also been measured and are shown in the Supporting Information.

Figure 5 reports the transient behavior of the photoJFET. We measure a rise time of ~10 μs, orders of magnitude faster than the fastest PbS CQD photoconductors previously reported (millisecond and above). Indeed, the combination of gain approaching 10 and response speed of approximately 100 kHz represents by far the fastest response time of a CQD photodetector exhibiting significant gain and low dark current.

CONCLUSIONS

In conclusion, the present work reports a novel CQD-based light sensor that enters a new regime of performance adjudged using the three crucial figures of merit of gain, speed, and background current. This device differs from previously reported CQD-based phototransistors,[32] which provided transport in a separate medium (such as graphene or MoS_2[33]). Instead, the photoJFET absorbs and transports in a single medium and exploits the photogate to modify the conductivity of the channel at zero bias; the junction gate-effect differentiates this phototransistor from the traditional metal–insulator–semiconductor (MIS) architecture.[34,35] Further improvements stand to be achieved by using more advanced lithographic definition to shorten the channel length to increase gain and reduce the volume of material producing thermal generation current across the reverse-biased junction in the dark; and by improving transport further in the channel to decrease transit time and increase speed of response and thus increase gain. As CQD-based rectifying metal–semiconductor junctions and heterojunctions are further improved, the Schottky device used to fully deplete the photoJFET in the dark stands to be enhanced further with the goal of minimizing interfacial recombination and consequent leakage current.

METHODS

Materials Preparation. Colloidal quantum dots were synthesized according to a previously published method.[36]

Sample Fabrication. A glass substrate with predeposited silver interdigitated electrodes was cleaned using acetone, isopropanol, and deionized water. The PbS CQD layer was deposited by spin-casting. PbS CQDs dissolved in octane (50 mg/mL) were spin-cast for 10 s at a speed of 2500 rpm. Tetrabutylammonium iodide (TBAI) dissolved in methanol (10 mg/mL) was then deposited on the film for the ligand exchange, left to soak for 10 s, and the liquid in excess was removed by spinning. Finally methanol was deposited on the surface and removed by spinning. This exchange/rinse was repeated a second time. The quantum dot/exchange/rinse procedure was repeated layer by layer until the desired thickness (240–300 nm) was reached. Molybdenum trioxide (MoO_3) was deposited (40 nm) using vacuum thermal evaporation. The entire fabrication process was performed in a nitrogen-filled glovebox. The channel length and width were fixed to 2.5 μm and 3 mm, respectively.

***I–V* Measurements.** Current–voltage measurements were performed using a Keithley 2400 source meter. The instrument was connected to the sample through triaxial cables and Cascade microprobe. These measurements were performed in an inert (N_2) environment.

Gain Measurements. Two methods were used to measure the gain of the detector as previously reported.[14] In the first method, a Keithley 2400 was used to measure the dark current and the photocurrent. The incident light power, produced by a narrow bandwidth OSRAM LED (λ = 450 nm), was measured using a calibrated Newport 1830c power meter, by integrating the intensity profile of the beam, passing through an aperture, over the device active area. The detector was put in direct contact with the aperture. The net photogenerated current was divided by the incident light power and multiplied by a factor hf/q. In the second method, a load resistor was connected in series with the

photodetector, and a bias voltage was provided by the Keithley 2400 source meter. The voltage drop across the load resistor, produced by the photocurrent, was measured using a SR830 Stanford Research lock-in amplifier that also allowed for noise measurements. When performing lock-in measurements, the monochromatic illumination was provided by combining a solar simulator and a monochromator. All of these measurements were realized in a dark and inert (N_2) environment.

Spectral Photocurrent Measurements. Monochromatic excitation was provided by using a 450 W Horiba Jobin-Yvon xenon arc Lamp and monochromator system. Appropriate order sorting filters (Newport) were used, and the incident power was kept constant at each wavelength using a neutral density filter. The photoJFET was biased using a Keithley 2400 source meter. The photocurrent was measured using a Stanford Research Systems SR830 lock-in amplifier. The light excitation was modulated using a mechanical chopper.

Speed Measurements. A monochromatic (λ = 450 nm) excitation, with a power of 140 μW, was provided by an LED driven by a function generator. The output signal from the photodetector, biased using a Keithley 2400 source meter, was amplified using a Stanford Research Systems SR570 current preamplifier and acquired with an Agilent Infiniium DSO 84 digital oscilloscope.

Conflict of Interest: The authors declare no competing financial interest.

Supporting Information Available: Colloidal quantum dot film absorbance, analytical model, fall and rise time, junction rectification, responsivity, spectral gain, carrier lifetime, mobility and gain estimation, detectivity, and noise current. This material is available free of charge via the Internet at http://pubs.acs.org.

Acknowledgment. The authors would like to acknowledge E. Palmiano, R. Wolowiec, and D. Kopilovic for technical assistance and guidance. Thanks to C. Maragliano for the valuable discussions. This publication is based in part on work supported by Award KUS-11-009-21 made by King Abdullah University of Science and Technology (KAUST), by the Ontario Research Fund—Research Excellence Program, and by the Natural Sciences and Engineering Research Council (NSERC) of Canada.

REFERENCES AND NOTES

1. Soref, R. A. Silicon-Based Optoelectronics. *Proc. IEEE* **1993**, *81*, 1687–1706.
2. Shen, Y. C.; Upadhya, P. C.; Linfield, E. H.; Beere, H. E.; Davies, A. G. Ultrabroadband Terahertz Radiation from Low-Temperature-Grown GaAs Photoconductive Emitters. *Appl. Phys. Lett.* **2003**, *83*, 3117.
3. Ito, H.; Furuta, T.; Kodama, S.; Ishibashi, T. InP/InGaAs Uni-Travelling-Carrier Photodiode with 310 GHz Bandwidth. *Electron. Lett.* **2000**, *36*, 1809.
4. Greiner, M. T.; Helander, M. G.; Wang, Z. B.; Tang, W. M.; Qiu, J.; Lu, Z. H. A Metallic Molybdenum Suboxide Buffer Layer for Organic Electronic Devices. *Appl. Phys. Lett.* **2010**, *96*, 213302.
5. Wu, S.; Li, W.; Chu, B.; Lee, C. S.; Su, Z.; Wang, J.; Yan, F.; Zhang, G.; Hu, Z.; Zhang, Z. High Response Deep Ultraviolet Organic Photodetector with Spectrum Peak Focused on 280 Nm. *Appl. Phys. Lett.* **2010**, *96*, 093302.
6. Morimune, T.; Kajii, H.; Ohmori, Y. Photoresponse Properties of a High-Speed Organic Photodetector Based on Copper–Phthalocyanine Under Red Light Illumination. *IEEE Photonics Technol. Lett.* **2006**, *18*, 2662–2664.
7. Talapin, D. V.; Murray, C. B. PbSe Nanocrystal Solids for N- and P-Channel Thin Film Field-Effect Transistors. *Science* **2005**, *310*, 86–89.
8. Guyot-Sionnest, P. Colloidal Quantum Dots. *C. R. Phys.* **2008**, *9*, 777–787.
9. Gao, J.; Luther, J. M.; Semonin, O. E.; Ellingson, R. J.; Nozik, A. J.; Beard, M. C. Quantum Dot Size Dependent J-V Characteristics in Heterojunction ZnO/PbS Quantum Dot Solar Cells. *Nano Lett.* **2011**, *11*, 1002–1008.
10. Oertel, D. C.; Bawendi, M. G.; Arango, A. C.; Bulović, V. Photodetectors Based on Treated CdSe Quantum-Dot Films. *Appl. Phys. Lett.* **2005**, *87*, 213505.
11. Clifford, J. P.; Konstantatos, G.; Johnston, K. W.; Hoogland, S.; Levina, L.; Sargent, E. H. Fast, Sensitive and Spectrally Tuneable Colloidal-Quantum-Dot Photodetectors. *Nat. Nanotechnol.* **2009**, *4*, 40–44.
12. Choudhury, K. R.; Sahoo, Y.; Ohulchanskyy, T. Y.; Prasad, P. N. Efficient Photoconductive Devices at Infrared Wavelengths Using Quantum Dot-Polymer Nanocomposites. *Appl. Phys. Lett.* **2005**, *87*, 073110.
13. Kim, S.; Mohseni, H.; Erdtmann, M.; Michel, E.; Jelen, C.; Razeghi, M. Growth and Characterization of InGaAs/InGaP Quantum Dots for Midinfrared Photoconductive Detector. *Appl. Phys. Lett.* **1998**, *73*, 963.
14. Konstantatos, G.; Howard, I.; Fischer, A.; Hoogland, S.; Clifford, J.; Klem, E.; Levina, L.; Sargent, E. H. Ultrasensitive Solution-Cast Quantum Dot Photodetectors. *Nature* **2006**, *442*, 180–183.
15. Konstantatos, G.; Clifford, J.; Levina, L.; Sargent, E. H. Sensitive Solution-Processed Visible-Wavelength Photodetectors. *Nat. Photonics* **2007**, *1*, 531–534.
16. Jeong, S. Y.; Lim, S. C.; Bae, D. J.; Lee, Y. H.; Shin, H. J.; Yoon, S.-M.; Choi, J. Y.; Cha, O. H.; Jeong, M. S.; Perello, D. Photocurrent of CdSe Nanocrystals on Single-Walled Carbon Nanotube-Field Effect Transistor. *Appl. Phys. Lett.* **2008**, *92*, 243103.
17. Klekachev, A. V.; Asselberghs, I.; Kuznetsov, S. N.; Cantoro, M.; Mun, J. H.; Cho, B.-J.; Hotta, J.; Hofkens, J.; van der Veen, M.; Stesmans, A. L.; *et al.* Charge Transfer Effects in Graphene-CdSe/ZnS Quantum Dots Composites. In *SPIE NanoScience + Engineering*; Pribat, D., Lee, Y.-H., Razeghi, M., Eds.; International Society for Optics and Photonics: Bellingham, WA, 2012; p 84620L.
18. Yang, S.; Zhao, N.; Zhang, L.; Zhong, H.; Liu, R.; Zou, B. Field-Effect Transistor-Based Solution-Processed Colloidal Quantum Dot Photodetector with Broad Bandwidth into near-Infrared Region. *Nanotechnology* **2012**, *23*, 255203.
19. Konstantatos, G.; Badioli, M.; Gaudreau, L.; Osmond, J.; Bernechea, M.; Garcia de Arquer, F. P.; Gatti, F.; Koppens, F. H. L. Hybrid Graphene-Quantum Dot Phototransistors with Ultrahigh Gain. *Nat. Nanotechnol.* **2012**, *7*, 363–368.
20. Sun, Z.; Liu, Z.; Li, J.; Tai, G.-A.; Lau, S.-P.; Yan, F. Infrared Photodetectors Based on CVD-Grown Graphene and PbS Quantum Dots with Ultrahigh Responsivity. *Adv. Mater.* **2012**, *24*, 5878–5883.
21. Hartgring, C. D. An Accurate JFET/MESFET Model for Circuit Analysis. *Solid. State. Electron.* **1982**, *25*, 233–240.
22. Brown, P. R.; Lunt, R. R.; Zhao, N.; Osedach, T. P.; Wanger, D. D.; Chang, L.-Y.; Bawendi, M. G.; Bulović, V. Improved Current Extraction from ZnO/PbS Quantum Dot Heterojunction Photovoltaics Using a MoO3 Interfacial Layer. *Nano Lett.* **2011**, *11*, 2955–2961.
23. Sahni, S.; Luo, X.; Liu, J.; Xie, Y.; Yablonovitch, E. Junction Field-Effect-Transistor-Based Germanium Photodetector on Silicon-on-Insulator. *Opt. Lett.* **2008**, *33*, 1138–1140.
24. Wang, X.; Koleilat, G. I.; Tang, J.; Liu, H.; Kramer, I. J.; Debnath, R.; Brzozowski, L.; Barkhouse, D. A. R.; Levina, L.; Hoogland, S.; *et al.* Tandem Colloidal Quantum Dot Solar Cells Employing a Graded Recombination Layer. *Nat. Photonics* **2011**, *5*, 480–484.
25. Shin, W.-J.; Lee, J.-Y.; Kim, J. C.; Yoon, T.-H.; Kim, T.-S.; Song, O.-K. Bulk and Interface Properties of Molybdenum Trioxide-Doped Hole Transporting Layer in Organic Light-Emitting Diodes. *Org. Electron.* **2008**, *9*, 333–338.
26. Tokito, S.; Noda, K.; Taga, Y. Metal Oxides as a Hole-Injecting Layer for an Organic Electroluminescent Device. *J. Phys. D: Appl. Phys.* **1996**, *29*, 2750–2753.
27. Zhitomirsky, D.; Furukawa, M.; Tang, J.; Stadler, P.; Hoogland, S.; Voznyy, O.; Liu, H.; Sargent, E. H. N-Type Colloidal-Quantum-Dot Solids for Photovoltaics. *Adv. Mater.* **2012**, *24*, 6181–6185.
28. Muñoz, E.; Monroy, E.; Garrido, J. A.; Izpura, I.; Sánchez, F. J.; Sánchez-García, M. A.; Calleja, E.; Beaumont, B.; Gibart, P. Photoconductor Gain Mechanisms in GaN Ultraviolet Detectors. *Appl. Phys. Lett.* **1997**, *71*, 870.
29. Adinolfi, V.; Ning, Z.; Xu, J.; Masala, S.; Zhitomirsky, D.; Thon, S. M.; Sargent, E. H. Electric Field Engineering Using

Quantum-Size-Effect-Tuned Heterojunctions. *Appl. Phys. Lett.* **2013**, *103*, 011106.
30. Konstantatos, G.; Sargent, E. H. Nanostructured Materials for Photon Detection. *Nat. Nanotechnol.* **2010**, *5*, 391–400.
31. Konstantatos, G.; Levina, L.; Fischer, A.; Sargent, E. H. Engineering the Temporal Response of Photoconductive Photodetectors via Selective Introduction of Surface Trap States. *Nano Lett.* **2008**, *8*, 1446–1450.
32. Ghosh, S.; Hoogland, S.; Sukhovatkin, V.; Levina, L.; Sargent, E. H. A Tunable Colloidal Quantum Dot Photo Field-Effect Transistor. *Appl. Phys. Lett.* **2011**, *99*.
33. Kufer, D.; Nikitskiy, I.; Lasanta, T.; Navickaite, G.; Koppens, F. H. L.; Konstantatos, G. Hybrid 2D-0D MoS_2-PbS Quantum Dot Photodetectors. *Adv. Mater.* **2015**, *27* (1), 176–180.
34. Xue, D.-J.; Wang, J.-J.; Wang, Y.-Q.; Xin, S.; Guo, Y.-G.; Wan, L.-J. Facile Synthesis of Germanium Nanocrystals and Their Application in Organic-Inorganic Hybrid Photodetectors. *Adv. Mater.* **2011**, *23*, 3704–3707.
35. Shieh, J.-M.; Yu, W.-C.; Huang, J. Y.; Wang, C.-K.; Dai, B.-T.; Jhan, H.-Y.; Hsu, C.-W.; Kuo, H.-C.; Yang, F.-L.; Pan, C.-L. Near-Infrared Silicon Quantum Dots Metal-Oxide-Semiconductor Field-Effect Transistor Photodetector. *Appl. Phys. Lett.* **2009**, *94*, 241108.
36. Hines, M. A.; Scholes, G. D. Colloidal PbS Nanocrystals with Size-Tunable Near-Infrared Emission: Observation of Post-Synthesis Self-Narrowing of the Particle Size Distribution. *Adv. Mater.* **2003**, *15*, 1844–1849.